ACS central science

http://pubs.acs.org/journal/acscii

Research Article

Large-Scale Production of Hierarchically Porous Metal–Organic Frameworks by a Reflux-Assisted Post-Synthetic Ligand Substitution Strategy

Guorui Cai,[†] Xing Ma,[†] Meruyert Kassymova, Kang Sun, Meili Ding, and Hai-Long Jiang*

Cite This: *ACS Cent. Sci.* 2021, 7, 1434–1440

Read Online

ACCESS | Metrics & More | Article Recommendations | Supporting Information

ABSTRACT: The mass production of hierarchically porous metal–organic frameworks (HP-MOFs) with adjustable morphology and size as well as retained crystallinity is highly desirable yet challenging. Herein, we have developed a versatile post-synthetic ligand substitution (PSLS) strategy to convert typical microporous MOFs and even their composites to HP-MOFs and their composites at a 10 g level and beyond in a simple reflux system. The resulting HP-MOFs feature intrinsic micropores and abundant defective mesopores, which greatly facilitate the transport and activation of large substrates for stable and efficient heterogeneous catalysis. Furthermore, the presence of defective mesopores in the HP-MOF composites improves activity and selectivity for large molecule-involved one-pot tandem catalysis. This strategy opens a new door to fast, facile, general, and scale-up production of HP-MOFs and related composites for expanding applications of conventional microporous MOF-based materials.

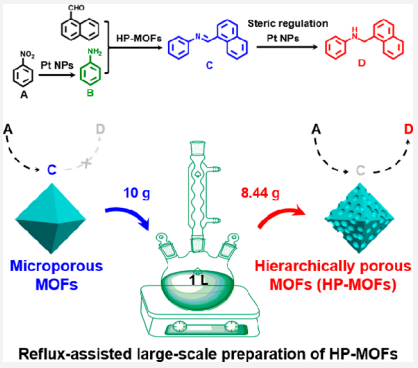

INTRODUCTION

Metal–organic frameworks (MOFs) as a relatively new class of crystalline porous solids have been widely accepted as a promising materials platform in many fields, benefiting from their high porosity and well-defined and tailored porous structures.[1−12] Their intrinsic micropores endow the particular capability of size-sieving and small molecule access, which are of importance in diverse applications. Nevertheless, in many cases, the small pores limit their applications involving large molecules.[13−17] A straightforward solution to the above issues is the extension of the bridging ligand length to afford mesoporous MOFs.[18−22] Unfortunately, the targeted products with high porosity are mostly thermodynamically instable and framework interpenetration is hardly avoidable.[18−22] Moreover, the long and complex organic linkers are usually insoluble and commercially unavailable, posing synthetic challenges. Alternatively, it is possible to introduce larger pores into parent microporous MOFs, producing hierarchically porous MOFs (HP-MOFs).[23] The intrinsic micropores conduce to high surface area and abundant active sites, while the introduced mesopores or macropores across the microporous matrix would facilitate the diffusion and transport of substrates and/or products, which significantly extend their application potentials and enhance their performance. To achieve this target, some in situ synthetic methods have been developed to fabricate HP-MOFs, on the basis of soft/hard template, nontemplate, ligand fragment, modulator-assisted strategies, etc.[24−38] The key point of these methods is to explore special templating reagents (hard template, soft surfactant, defective ligand, or special modulator), which not only possess special interaction with the MOF skeleton to create the large pores but also can be removed subsequently without disrupting the overall MOF structure. Accordingly, the increased process complexity and/or high cost are usually unavoidable, making it difficult for large-scale synthesis toward real-world applications.[39]

In this context, the introduction of meso/macropores into intrinsically microporous MOFs by a post-treatment process would be a promising strategy that meets the practical demands. Although several related studies, such as heat treatment, acid/alkali etching, etc., have been reported;[40−47] unfortunately, the harsh chemical/thermal treatments often damage their pristine MOF structures and even introduce some impurities, such as metal oxides.[40,41] Moreover, the etching/destruction of the parent MOF structures is hard to control, which places high demand on particular etching reagents and MOF stability. Therefore, a simple, fast, general, and scalable synthetic approach to the conversion of microporous MOFs into hierarchically porous structures remains imperative.

The post-synthetic ligand exchange (PSE, named by Kim et al.[48]) has been widely used to introduce functionalized ligands into MOFs under mild conditions, where a new bridging ligand

Received: June 22, 2021
Published: August 6, 2021

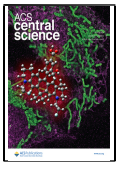

https://doi.org/10.1021/acscentsci.1c00743
ACS Cent. Sci. 2021, 7, 1434–1440

is generally used to replace the pre-existing ligand of MOFs while preserving the bulk crystallinity.[11,48−52] Inspired by this mild conversion process, we describe a facile post-synthetic ligand substitution (PSLS) strategy by substituting the bridging ligand in microporous MOFs with a terminal ligand to create additional defective spaces, which is a mild process without an obvious disruption of the morphology and size of the parent MOF particles. The mesopores and even macropores can be generated and tailored to afford HP-MOFs by simply controlling the ratio/amount of terminal ligand (Figure 1). The HP-MOFs with different structural topologies,

Figure 1. Schematic showing the conversion of microporous MOFs into corresponding hierarchically porous structures on the basis of the PSLS strategy.

including UiO-66 with different sizes and morphologies,[53] UiO-67,[53] MOF-808,[54] and MIL-53,[55] can be produced (Figure S1), demonstrating the good generality of this strategy. This reflux-assisted process is very easy to operate and scale up to at least 10 g in one pot.[56] The resultant HP-MOFs not only feature intrinsic micropores enriching small-size substrates and meso-/macro-pores entrapping large functional species but also possess abundant defective sites, which are able to interact and activate substrates. The CO_2 cycloaddition of epoxides and one-pot cascade hydrogenation/condensation reactions have been conducted, as a proof-of-concept, highlighting the collaborative strengths of ordered micropores and defective mesopores toward efficient and selective catalysis.

RESULTS AND DISCUSSION

Given its high chemical and thermal stability, the well-known microporous MOF, UiO-66, was first selected as a representative model for the PSLS study. Typically, the UiO-66 powder was introduced into an aqueous solution of sodium acetate, followed by a reflux treatment at 100 °C to promote the ligand substitution process (Figure 1, Supporting Information, Section S2.2). Upon activation in *N*,*N*-dimethylformamide (DMF) solution with hydrochloric acid to remove the residual ligands in MOF pores, hierarchically porous UiO-66 (denoted HP-UiO-66) was obtained. It is worth noting that, in contrast to the conventional solvothermal synthesis in an autoclave, this PSLS process by refluxing treatment in a flask is very simple and promising for conversion in a large scale. Mass production can be achieved by simply using a large-volume flask. As a laboratory demonstration, we have successfully completed the conversion of 10 g of MOFs (HP-MOF yield: 8.44 g) in a 1 L flask (Figure 2a−c).

Nitrogen sorption measurements indicate that the pristine UiO-66 possesses a high microporosity with a pore volume of 0.52 cm^3/g. After the post-synthesis conversion, the resulting HP-MOF exhibits an increased total pore volume (0.68 cm^3/g) with the introduction of mesopores, while only a slightly decreased specific BET surface area (S_{BET}) compared with that of their pristine MOFs (S_{BET}: 802 vs 995 m^2g^{-1}). The pore size

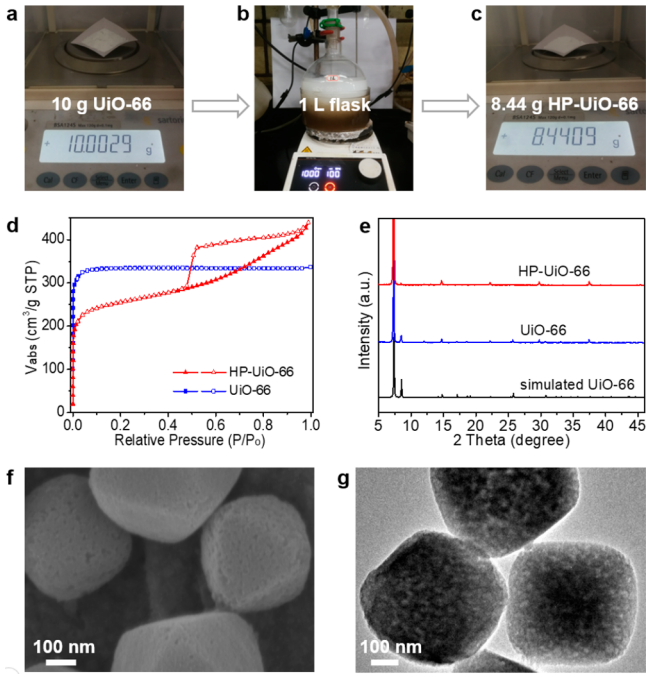

Figure 2. (a−c) Experimental photos of reflux setup (1 L) showing the scale-up conversion of UiO-66 into HP-UiO-66 in one pot. (d) N_2 sorption isotherms at 77 K and (e) powder XRD patterns of UiO-66 and HP-UiO-66. (f) SEM and (g) TEM images of HP-UiO-66.

distribution data show that the intrinsic micropores (<2 nm) in MOFs are basically maintained, while mesoporous features (2−20 nm) clearly appear after the PSLS process (Figure 2d and Figure S2). Powder X-ray diffraction (XRD) patterns show that no noticeable decrease in the crystallinity occurred after this mild PSLS process (Figure 2e). Scanning electron microscopy (SEM) images show that the morphology and size of UiO-66 particles are mostly maintained (Figure 2f and Figure S3). From both SEM and transmission electron microscopy (TEM) images, the additional mesopores are observable in HP-UiO-66 (Figure 2g). The above results unambiguously demonstrate that this strategy is able to create additional mesopores while keeping UiO-66 structure, microporosity, particle size, and morphology, which is highly desired for various practical applications.

A series of control experiments have been attempted to figure out the real role of sodium acetate in the mesopore generation of HP-UiO-66. In view of the fact that the hydrolysis of sodium acetate would produce hydroxide ion (OH^-), whether the mesopore formation related to the OH^- etching should be checked. However, this concern is ruled out by employing a neutral strong electrolyte, ammonium acetate, by which a similar hierarchically porous structure can be obtained (Figure S4). This point is further evidenced by using NaOH solution to etch UiO-66; no additional pore can be generated even under the same pH as the aqueous solution of sodium acetate (Figure S5). Similarly, when post-treating with the same molar amount of aqueous acetic acid, no additional pore can be produced (Figure S6). This result is probably attributed to the weak electrolyte feature of acetic acid (higher pK_a than terephthalic acid), which, dissociation in only a slight degree, is not able to provide sufficient acetate ions to drive the PSLS process. As expected, when the weak carboxylic acid is replaced by corresponding carboxylates, such as sodium

https://doi.org/10.1021/acscentsci.1c00743
ACS Cent. Sci. 2021, 7, 1434−1440

formate, sodium propionate, sodium benzoate, etc., the conversion to HP-UiO-66 can be successfully achieved after this PSLS process (Figures S7−S9). To unveil the mechanism, some carboxylates with a long chain are deliberately used; the steric resistance stemmed from the MOF micropores suppresses the entrance of these bulky carboxylates. As a result, only the marginal layer of the MOF particles can be etched, while no noticeable mesopores and structural change can be found in the MOF interior (Figures S10 and S11). However, if sodium acetate was directly added in the synthetic system of conventional UiO-66, no crystalline UiO-66 can be obtained (Figure S12), ruling out the possibility of in situ defective mesopore formation accompanied by the MOF assembly.

To elucidate the influence of the terminal ligand amount on the substitution process, 0, 2, 4, 6, 8, or 10 mmol of sodium acetate was used in the synthesis of HP-UiO-66. As indicated in N_2 sorption curves (Figure S13), a small amount of terminal ligand does not cause the change in the pore feature of UiO-66. The mesoporous characteristics, i.e., hysteresis loop in N_2 sorption curves, start to appear by increasing the sodium acetate amount to 4 mmol. A further increased concentration of sodium acetate results in the gradual increase of mesoporosity. Accordingly, the mesoporous behavior can be tuned by changing the amount of the terminal ligand. However, most of the UiO-66 skeleton is etched away when the concentration of sodium acetate is too high, resulting in structural collapse. All these results jointly suggest that both concentration and size of carboxylate play key roles in this PSLS process. In addition, it is noteworthy that the introduction of polyvinylpyrrolidone (PVP) in the sodium acetate aqueous solution is necessary to promote the formation of mesopores while maintaining a high pristine microporosity (Figure S14a). Moreover, the difference between the TEM images (Figure 2g and Figure 14b) and the similar high yields (88.5%−92.9%) of HP-UiO-66 obtained with different amounts of PVP indicate that the PVP might mainly influence the distribution of the acetate to etch the MOF,[51] not the etching rate/reaction equilibrium. Therefore, we propose that the PVP might behave as the protective coating to prevent the destruction of the MOF particle surface during the diffusion of etchant (acetate) into the MOF interior, thereby promoting the production of homogeneous mesopores in the entire MOF particles (Figure 2g).

The UiO-66 before and after PSLS process have been characterized by ^{1}H NMR. Results show that the treated MOFs present some characteristic peaks assignable to the acetate, and these peaks disappear after activation treatment (Figure 3a). The ratio of acetate/1,4-benzenedicarboxylate (BDC) calculated by integral area of ^{1}H NMR peaks in HP-UiO-66 before HCl activation is obviously higher than those in conventional UiO-66, indicating a higher degree of defect in the former (0.33 vs 0.10; Figure S15). Furthermore, the FT-IR peak at 2975 cm^{-1} assignable to the saturated alkane appears after the PSLS treatment and disappears after activation, indicating the successful substitution of acetate into the MOF skeleton and subsequent removal in the activation process (Figure S16). To gain visual evidence on the mesopore generation, the resulting HP-UiO-66 was soaked into dye solutions with different charges. While the anionic dyes (methyl orange, MO) can be absorbed, the cationic dyes (methylene blue, MB) are hardly captured (Figure 3b,c), indicating the cationic framework due to the missing of linkers.

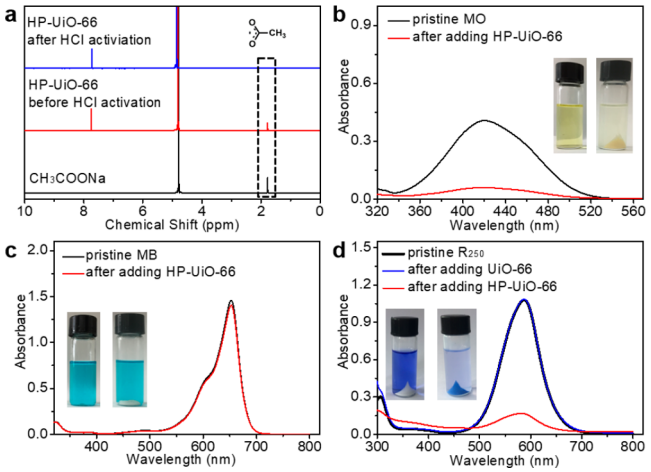

Figure 3. (a) ^{1}H NMR spectra for CH_3COONa and HP-UiO-66 before and after activation. UV/vis absorption spectra recording the adsorption of (b) small-sized anionic dye (MO), (c) small-sized cationic dye (MB), and (d) large-sized anionic dye (R_{250}) by UiO-66 and HP-UiO-66. Insets in b and c: photos of dye solution (left) before and (right) after adding HP-UiO-66. Insets in d: photos of dye solution after adding (left) UiO-66 and (right) HP-UiO-66.

When soaking HP-UiO-66 in a DMF solution of Coomassie Brilliant Blue R_{250} (R_{250}), the solution gradually fades and the white HP-UiO-66 accordingly turns to brilliant blue (Figure 3d). In stark contrast, due to the larger size of R_{250} than the micropore opening, the pristine UiO-66 is not able to uptake R_{250} and thus its color remains unchanged even after longer soaking time. This clear comparison again manifests the presence of defective mesopores in HP-UiO-66. Altogether, the above information unambiguously supports that the acetate coordinates to the Zr-oxo clusters, creating the structural defects, and subsequently, it can be removed to release the mesoporous space after activation.

Systematic characterizations have been conducted to figure out the function of the (DMF + aqueous HCl) treatment in the activation process. To evaluate if there are Cl^- ions in the activated HP-UiO-66, the content of Cl^- ions in the suspension of HP-UiO-66 dissolved by NaOH aqueous solution has been detected by ion chromatography, which indicates a Cl^- ion content of 17 $\mu g/mg_{HP\text{-}UiO\text{-}66}$. Moreover, the obvious Cl 2p signal peak at 198.2 eV in the X-ray photoelectron spectroscopy (XPS) spectrum can be identified in the activated HP-UiO-66, suggesting the charge balance role of Cl^- ion in the defective MOF structure (Figure S17).[57] In addition, the TGA curves of HP-UiO-66 before and after the (DMF + aqueous HCl) treatment pose an obvious deviation on the mass drop below 150 °C (Figure S18). The increased mass drop in the activated HP-UiO-66 can be attributed to physiosorbed/coordinated H_2O proven by the OH stretch peaks (~3400 cm^{-1}) in the FTIR spectrum (Figure S16). Therefore, we propose that the coordinated acetate was removed by the (DMF + aqueous HCl) activation, which causes a chlorine containing MOF (Figure S19).[58−60]

In addition, the Zr content in the above two solutions was detected by inductively coupled plasma atomic emission spectrometer (ICP-AES), which indicates that the Zr concentrations are 1.44 and 0.01 mg/mL, respectively, in the sodium acetate reflux solution and the (DMF + aqueous HCl) activation solution. The high concentration of Zr in the former indicates that UiO-66 is etched by acetate and thus the

https://doi.org/10.1021/acscentsci.1c00743
ACS Cent. Sci. 2021, 7, 1434−1440

formation of mesopores. To evaluate if the (DMF + aqueous HCl) treatment would further etch the MOF structure and introduce additional mesopores, the same treatment was performed on the pristine UiO-66 powder. All characterizations demonstrate that no mesoporous feature can be identified (Figure S20). In addition, both UiO-66 and HP-UiO-66 are stable even in concentrated HCl (Figure S21). The above results indicate that the low concentration of Zr in the (DMF + aqueous HCl) solution is not caused from the further etching of the HP-UiO-66 skeleton by HCl. It might come from the Zr residual in the MOF pores formed in the acetate reflux process.

With the above results, we hypothesize that the PSLS might be a reversible process in the generation of HP-UiO-66, on the basis of the equilibrium of dissociation and reassembly (Figure 4a).[48−52] Upon soaking MOF crystals into the terminal ligand

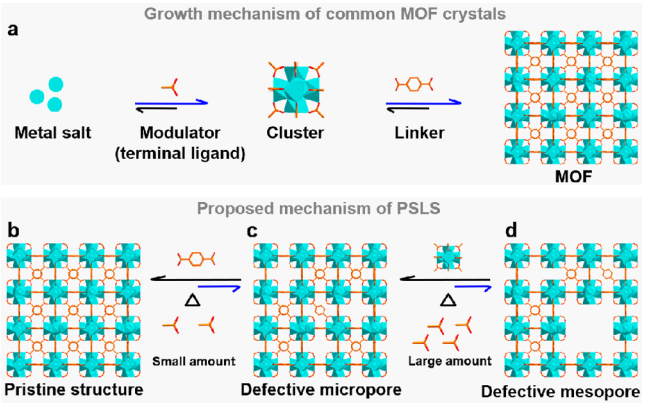

Figure 4. (a) Typical growth mechanism of common MOF crystals. (b−d) Proposed mechanism for the typical conversion of a microporous MOF into hierarchically porous structure with different levels of structural defect on the basis of the PSLS strategy.

solution with high concentration, the equilibrium state of the pristine MOF would be broken. As a result, some linkers in the MOFs will be substituted by the terminal ligands after reaching a kinetic equilibrium state and thus producing small defective pores (Figure 4b,c). If the terminal ligand concentration in the solution is further increased, the above equilibrium state would be broken and pushed to another new kinetic equilibrium state. Along with an increased amount of terminal ligand, the bridging ligands around the metal cluster are gradually substituted, and even the metal cluster will be simultaneously released from the MOF matrix, resulting in a larger pore space (Figure 4c,d). On the basis of this mechanism, the etching extent of MOF skeleton can be controlled to generate different ranges of pores by using carboxylate as the terminal ligand. The terminal ligands coordinated to the metal-oxo clusters can be removed to afford the coordinatively unsaturated metal centers, behaving Lewis acid sites as discussed below, in the HP-MOFs after the activation process.

On the basis of the above mechanism, the generality of this conversion strategy has been investigated. Taking UiO-66 as a representative, HP-UiO-66 with different sizes (typical examples, 800 nm, 2 μm) and morphologies (in octahedral, dodecahedral, or cubic shape) can be obtained, depending on the original geometry of their parent MOFs (Figures S22−S29). Other types of MOFs, such as UiO-67, MIL-53, and MOF-808, featuring even completely different structures and compositions, have also been attempted. Encouragingly, they all can be converted into their corresponding hierarchically porous structures (denoted HP-UiO-67, HP-MIL-53, and HP-MOF-808, respectively) (Figures S30−S32). In view of the operation simplicity of this refluxing process followed by activation process, both of which are realized by stirring the sample in a flask, it is expected to achieve a large volume of HP-MOFs in one pot. To demonstrate this scale-up potential in the laboratory, when a 10-g-scale conversion (100 times of magnification vs typical experiment) was attempted in a 1 L flask, 8.44 g of HP-MOFs was harvested (Figure 2a−c). The obtained HP-UiO-66 is uniform in its size and microstructure (Figures S33 and S34), similar to those in common-scale synthesis (Figure S3). In addition, the same PSLS process has been applied for preparing MOF-based composites. Taking UiO-66 encapsulating platinum nanoparticles (denoted Pt@UiO-66) as an example, to our delight, which can be successfully converted into the corresponding composite featuring hierarchical pores (denoted Pt@HP-UiO-66, Figures S35−S38). It is believed that this is a highly general approach, and predictably, a variety of MOF-based composites featuring hierarchical pores can be achieved in mass production on the basis of this conversion strategy, which is definitely promising for broad and practical applications.

Given the unique hierarchical structures, these micropores and mesopores would synergistically promote catalytic reactions, where micropores expose active sites and enrich substrates while the defective mesopores benefit the rapid transport of substrates and provide a large number of open Zr sites as the Lewis acid sites (Figures S39−S42). As a proof of example, UiO-66 and HP-UiO-66 have been employed for the catalytic CO_2 cycloaddition of epoxides, upgrading CO_2 to high-value products (Figure 5a,b).[61−63] The better mass transfer capability together with a higher concentration of defect sites in HP-UiO-66 are responsible for its significantly higher activity than the parent UiO-66. The conversion of various epoxides with different sizes illustrates the advantage and high activity of HP-UiO-66, particularly in large-size

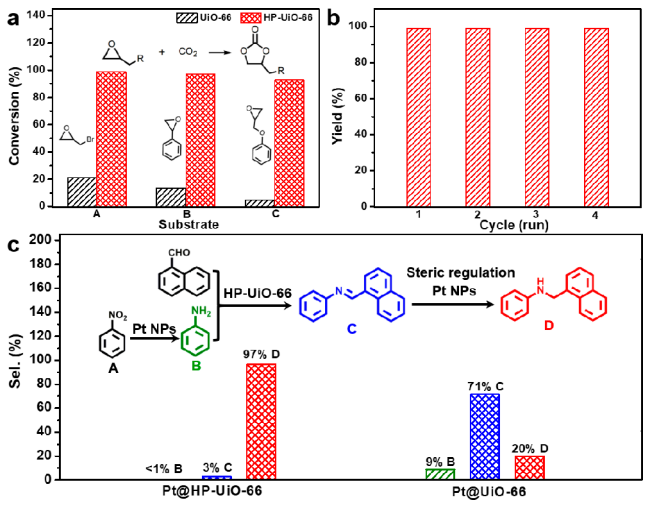

Figure 5. (a) Catalytic cycloaddition reactions between CO_2 and epoxides with different sizes on the basis of UiO-66 and HP-UiO-66 catalysts. (b) Recycling test of the CO_2 cycloaddition with epibromohydrin over HP-UiO-66. (c) One-pot cascade synthesis of secondary arylamines through the hydrogenation of nitrobenzene and the reductive amination of benzaldehyde reactions over Pt@UiO-66 and Pt@HP-UiO-66.

https://doi.org/10.1021/acscentsci.1c00743
ACS Cent. Sci. 2021, 7, 1434−1440

molecule involved mass transfer, far superior to microporous UiO-66 (Figure 5a).

Not limited to the enhanced activity of straightforward reactions, HP-MOFs are even able to promote complex reactions with both improved activity and selectivity. Taking Pt@HP-UiO-66 as an example, it exhibits particular strengths in one-pot multistep cascade reactions (Figure S43). The hierarchically porous composites can convert nitrobenzene (A) into *N*-(naphthalen-1-ylmethyl)aniline (D) in one-pot cascade reaction, with the selectivities of <1%, ∼ 3%, and ∼97% to aniline (B), *N*-phenylnaphthalene-1-(methanimine) (C), and D, respectively. In sharp contrast, their microporous composite mainly converted A into intermediate C with a selectivity ∼71%, and only a 20% selectivity to the D in the same reaction time length, due to the restrict effect of micropores on intermediate products (Figure 5c and Figure S44). All above clearly highlight the synergistic strengths of the ordered micropores and generated defective mesopores toward catalytic applications involving large-size substrates and products.

CONCLUSIONS

In summary, we have developed a simple yet highly effective and general strategy to the conversion of common microporous MOFs and their composites into their corresponding hierarchically porous structures. This conversion can be easily scaled up to 10 g and even higher amounts, during which the pristine MOF structure (and related micropores) can be maintained, while some structural domains are disassembled to create additional defective mesopores in resulting HP-MOFs. The incorporation of guest species inside MOF particles does not disturb this conversion and the synthetic strategy can be applicable to diverse MOF-based composites. With the cooperation of coexisted micropores and defective mesopores, the HP-MOFs and related composites greatly boost catalytic reactions and even multistep cascade reactions in one pot, exhibiting improved activity and selectivity in reference to the parent microporous MOF-based materials. This work opens a novel and general avenue to MOFs with hierarchical pores into mass production and pushes one-step forward for MOF-based materials toward broad and practical applications.

ASSOCIATED CONTENT

Supporting Information

The Supporting Information is available free of charge at https://pubs.acs.org/doi/10.1021/acscentsci.1c00743.

Discussions of materials and instrumentation used, experimental details, uptake of guest species, and catalytic activity evaluation and figures of crystal structures, pore size distributions, SEM and TEM images, N_2 sorption isotherms, powder XRD patterns, NMR spectra, FT-IR patterns, XPS spectra, thermogravimetric curves, proposed defective structures, CO_2 sorption isotherms, adsorption curve, proposed mechanisms, and recycling tests (PDF)

AUTHOR INFORMATION

Corresponding Author

Hai-Long Jiang − *Hefei National Laboratory for Physical Sciences at the Microscale, CAS Key Laboratory of Soft Matter Chemistry, Department of Chemistry, University of Science and Technology of China, Hefei, Anhui 230026, P. R. China*; orcid.org/0000-0002-2975-7977; Email: jianglab@ustc.edu.cn

Authors

Guorui Cai − *Hefei National Laboratory for Physical Sciences at the Microscale, CAS Key Laboratory of Soft Matter Chemistry, Department of Chemistry, University of Science and Technology of China, Hefei, Anhui 230026, P. R. China*

Xing Ma − *Hefei National Laboratory for Physical Sciences at the Microscale, CAS Key Laboratory of Soft Matter Chemistry, Department of Chemistry, University of Science and Technology of China, Hefei, Anhui 230026, P. R. China*

Meruyert Kassymova − *Hefei National Laboratory for Physical Sciences at the Microscale, CAS Key Laboratory of Soft Matter Chemistry, Department of Chemistry, University of Science and Technology of China, Hefei, Anhui 230026, P. R. China*

Kang Sun − *Hefei National Laboratory for Physical Sciences at the Microscale, CAS Key Laboratory of Soft Matter Chemistry, Department of Chemistry, University of Science and Technology of China, Hefei, Anhui 230026, P. R. China*

Meili Ding − *Hefei National Laboratory for Physical Sciences at the Microscale, CAS Key Laboratory of Soft Matter Chemistry, Department of Chemistry, University of Science and Technology of China, Hefei, Anhui 230026, P. R. China*

Complete contact information is available at: https://pubs.acs.org/10.1021/acscentsci.1c00743

Author Contributions

†G.C. and X.M. contributed equally to this work.

Notes

The authors declare no competing financial interest.

ACKNOWLEDGMENTS

This work was supported by the National Natural Science Foundation of China (21725101, 22161142001, and 21521001), the DNL Cooperation Fund, Chinese Academy of Sciences (DNL201911), and Fundamental Research Funds for the Central Universities (WK3450000007).

REFERENCES

(1) Zhao, X.; Wang, Y.; Li, D.-S.; Bu, X.; Feng, P. Metal-organic frameworks for separation. *Adv. Mater.* **2018**, *30*, 1705189.

(2) Zhou, H.-C.; Kitagawa, S. Metal-organic frameworks (MOFs). *Chem. Soc. Rev.* **2014**, *43*, 5415−5418.

(3) Li, B.; Wen, H.-M.; Cui, Y.; Zhou, W.; Qian, G.; Chen, B. Emerging multifunctional metal-organic framework materials. *Adv. Mater.* **2016**, *28*, 8819−8860.

(4) Kung, C.-W.; Goswami, S.; Hod, I.; Wang, T. C.; Duan, J.; Farha, O. K.; Hupp, J. T. Charge transport in zirconium-based metal-organic frameworks. *Acc. Chem. Res.* **2020**, *53*, 1187−1195.

(5) Li, G.; Zhao, S.; Zhang, Y.; Tang, Z. Metal-organic frameworks encapsulating active nanoparticles as emerging composites for catalysis: Recent progress and perspectives. *Adv. Mater.* **2018**, *30*, 1800702.

(6) Lustig, W. P.; Mukherjee, S.; Rudd, N. D.; Desai, A. V.; Li, J.; Ghosh, S. K. Metal-organic frameworks: functional luminescent and photonic materials for sensing applications. *Chem. Soc. Rev.* **2017**, *46*, 3242−3285.

(7) Jiao, L.; Wang, Y.; Jiang, H.-L.; Xu, Q. Metal-organic frameworks as platforms for catalytic applications. *Adv. Mater.* **2018**, *30*, 1703663.

(8) Dhakshinamoorthy, A.; Li, Z.; Garcia, H. Catalysis and photocatalysis by metal organic frameworks. *Chem. Soc. Rev.* **2018**, *47*, 8134−8172.

(9) Cui, W.-G.; Zhang, G.-Y.; Hu, T.-L.; Bu, X.-H. Metal-organic framework-based heterogeneous catalysts for the conversion of C_1 chemistry: CO, CO_2 and CH_4. *Coord. Chem. Rev.* **2019**, *387*, 79−120.
(10) Huang, G.; Yang, L.; Yin, Q.; Fang, Z.-B.; Hu, X.-J.; Zhang, A.-A.; Jiang, J.; Liu, T.-F.; Cao, R. A comparison of two isoreticular metal-organic frameworks with cationic and neutral skeletons: stability, mechanism, and catalytic activity. *Angew. Chem., Int. Ed.* **2020**, *59*, 4385−4390.
(11) Kalaj, M.; Cohen, S. M. Postsynthetic modification: an enabling technology for the advancement of metal-organic frameworks. *ACS Cent. Sci.* **2020**, *6*, 1046−1057.
(12) Li, K.; Yang, J.; Huang, R.; Lin, S.; Gu, J. Ordered large-pore mesoMOFs based on synergistic effects of triblock polymer and Hofmeister ion. *Angew. Chem., Int. Ed.* **2020**, *59*, 14124−14128.
(13) He, S.; Chen, Y.; Zhang, Z.; Ni, B.; He, W.; Wang, X. Competitive coordination strategy for the synthesis of hierarchical-pore metal-organic framework nanostructures. *Chem. Sci.* **2016**, *7*, 7101−7105.
(14) Jeoung, S.; Kim, S.; Kim, M.; Moon, H. R. Pore engineering of metal-organic frameworks with coordinating functionalities. *Coord. Chem. Rev.* **2020**, *420*, 213377.
(15) Li, P.; Modica, J. A.; Howarth, A. J.; Vargas, E.; Moghadam, P. Z.; Snurr, R. Q.; Mrksich, M.; Hupp, J. T.; Farha, O. K. Toward design rules for enzyme immobilization in hierarchical mesoporous metal-organic frameworks. *Chem* **2016**, *1*, 154−169.
(16) Meng, F.; Zhang, S.; Ma, L.; Zhang, W.; Li, M.; Wu, T.; Li, H.; Zhang, T.; Lu, X.; Huo, F.; et al. Construction of hierarchically porous nanoparticles@metal-organic frameworks composites by inherent defects for the enhancement of catalytic efficiency. *Adv. Mater.* **2018**, *30*, 1803263.
(17) Zhang, P.; Chen, C.; Kang, X.; Zhang, L.; Wu, C.; Zhang, J.; Han, B. In situ synthesis of sub-nanometer metal particles on hierarchically porous metal-organic frameworks via interfacial control for highly efficient catalysis. *Chem. Sci.* **2018**, *9*, 1339−1343.
(18) Deng, H.; Grunder, S.; Cordova, K. E.; Valente, C.; Furukawa, H.; Hmadeh, M.; Gándara, F.; Whalley, A. C.; Liu, Z.; Asahina, S.; et al. Large-pore apertures in a series of metal-organic frameworks. *Science* **2012**, *336*, 1018−1023.
(19) Jiang, H.-L.; Makal, T. A.; Zhou, H.-C. Interpenetration control in metal-organic frameworks for functional applications. *Coord. Chem. Rev.* **2013**, *257*, 2232−2249.
(20) Klein, N.; Senkovska, I.; Gedrich, K.; Stoeck, U.; Henschel, A.; Mueller, U.; Kaskel, S. A mesoporous metal-organic framework. *Angew. Chem., Int. Ed.* **2009**, *48*, 9954−9957.
(21) Li, T.; Kozlowski, M. T.; Doud, E. A.; Blakely, M. N.; Rosi, N. L. Stepwise ligand exchange for the preparation of a family of mesoporous MOFs. *J. Am. Chem. Soc.* **2013**, *135*, 11688−11691.
(22) Tan, C.; Han, X.; Li, Z.; Liu, Y.; Cui, Y. Controlled exchange of achiral linkers with chiral linkers in Zr-based UiO-68 metal-organic framework. *J. Am. Chem. Soc.* **2018**, *140*, 16229−16236.
(23) Cai, G.; Yan, P.; Zhang, L.; Zhou, H.-C.; Jiang, H.-L. Metal−Organic Framework-Based Hierarchically Porous Materials: Synthesis and Applications. *Chem. Rev.*, in press, **2021**.
(24) Zhao, Y.; Zhang, J.; Han, B.; Song, J.; Li, J.; Wang, Q. Metal-organic framework nanospheres with well-ordered mesopores synthesized in an ionic liquid/CO_2/surfactant system. *Angew. Chem., Int. Ed.* **2011**, *50*, 636−639.
(25) Cai, G.; Jiang, H.-L. A modulator-induced defect-formation strategy to hierarchically porous metal-organic frameworks with high stability. *Angew. Chem., Int. Ed.* **2017**, *56*, 563−567.
(26) Choi, K. M.; Jeon, H. J.; Kang, J. K.; Yaghi, O. M. Heterogeneity within order in crystals of a porous metal-organic framework. *J. Am. Chem. Soc.* **2011**, *133*, 11920−11923.
(27) Dissegna, S.; Epp, K.; Heinz, W. R.; Kieslich, G.; Fischer, R. A. Defective metal-organic frameworks. *Adv. Mater.* **2018**, *30*, 1704501.
(28) Kang, X.; Lyu, K.; Li, L.; Li, J.; Kimberley, L.; Wang, B.; Liu, L.; Cheng, Y.; Frogley, M. D.; Rudiü, S.; et al. Integration of mesopores and crystal defects in metal-organic frameworks via templated electrosynthesis. *Nat. Commun.* **2019**, *10*, 4466.
(29) Kirchon, A.; Li, J.; Xia, F.; Day, G. S.; Becker, B.; Chen, W.; Sue, H.-J.; Fang, Y.; Zhou, H.-C. Modulation versus templating: fine-tuning of hierarchally porous PCN-250 using fatty acids to engineer guest adsorption. *Angew. Chem., Int. Ed.* **2019**, *58*, 12425−12430.
(30) Li, K.; Lin, S.; Li, Y.; Zhuang, Q.; Gu, J. Aqueous-phase synthesis of mesoporous Zr-based MOFs templated by amphoteric surfactants. *Angew. Chem., Int. Ed.* **2018**, *57*, 3439−3443.
(31) Li, L.; Xiang, S.; Cao, S.; Zhang, J.; Ouyang, G.; Chen, L.; Su, C.-Y. A synthetic route to ultralight hierarchically micro/mesoporous Al(III)-carboxylate metal-organic aerogels. *Nat. Commun.* **2013**, *4*, 1774.
(32) Liang, W.; Li, L.; Hou, J.; Shepherd, N. D.; Bennett, T. D.; D'Alessandro, D. M.; Chen, V. Linking defects, hierarchical porosity generation and desalination performance in metal-organic frameworks. *Chem. Sci.* **2018**, *9*, 3508−3516.
(33) Park, J.; Wang, Z. U.; Sun, L.-B.; Chen, Y.-P.; Zhou, H.-C. Introduction of functionalized mesopores to metal-organic frameworks via metal-ligand-fragment coassembly. *J. Am. Chem. Soc.* **2012**, *134*, 20110−20116.
(34) Reboul, J.; Furukawa, S.; Horike, N.; Tsotsalas, M.; Hirai, K.; Uehara, H.; Kondo, M.; Louvain, N.; Sakata, O.; Kitagawa, S. Mesoscopic architectures of porous coordination polymers fabricated by pseudomorphic replication. *Nat. Mater.* **2012**, *11*, 717−723.
(35) Shen, K.; Zhang, L.; Chen, X.; Liu, L.; Zhang, D.; Han, Y.; Chen, J.; Long, J.; Luque, R.; Li, Y.; et al. Ordered macro-microporous metal-organic framework single crystals. *Science* **2018**, *359*, 206−210.
(36) Yue, Y.; Fulvio, P. F.; Dai, S. Hierarchical metal-organic framework hybrids: perturbation-assisted nanofusion synthesis. *Acc. Chem. Res.* **2015**, *48*, 3044−3052.
(37) Zhang, W.; Liu, Y.; Lu, G.; Wang, Y.; Li, S.; Cui, C.; Wu, J.; Xu, Z.; Tian, D.; Huang, W.; DuCheneu, J. S.; Wei, W. D.; Chen, H.; Yang, Y.; Huo, F. Mesoporous metal-organic frameworks with size-, shape-, and space-distribution-controlled pore structure. *Adv. Mater.* **2015**, *27*, 2923−2929.
(38) Cai, G.; Ding, M.; Wu, Q.; Jiang, H.-L. Encapsulating soluble active species into hollow crystalline porous capsules beyond integration of homogeneous and heterogeneous catalysis. *Natl. Sci. Rev.* **2020**, *7*, 37−45.
(39) Bradshaw, D.; El-Hankari, S.; Lupica-Spagnolo, L. Supramolecular templating of hierarchically porous metal-organic frameworks. *Chem. Soc. Rev.* **2014**, *43*, 5431−5443.
(40) Chen, S.; Mukherjee, S.; Lucier, B. E.; Guo, Y.; Wong, Y. A.; Terskikh, V. V.; Zaworotko, M. J.; Huang, Y. Cleaving carboxyls: understanding thermally triggered hierarchical pores in the metal-organic framework MIL-121. *J. Am. Chem. Soc.* **2019**, *141*, 14257−14271.
(41) Feng, L.; Yuan, S.; Zhang, L.-L.; Tan, K.; Li, J.-L.; Kirchon, A.; Liu, L.-M.; Zhang, P.; Han, Y.; Chabal, Y. J.; Zhou, H.-C. Creating hierarchical pores by controlled linker thermolysis in multivariate metal-organic frameworks. *J. Am. Chem. Soc.* **2018**, *140*, 2363−2372.
(42) Guillerm, V.; Xu, H.; Albalad, J.; Imaz, I.; Maspoch, D. Postsynthetic selective ligand cleavage by solid-gas phase ozonolysis fuses micropores into mesopores in metal-organic frameworks. *J. Am. Chem. Soc.* **2018**, *140*, 15022−15030.
(43) Koo, J.; Hwang, I.-C.; Yu, X.; Saha, S.; Kim, Y.; Kim, K. Hollowing out MOFs: hierarchical micro-and mesoporous MOFs with tailorable porosity via selective acid etching. *Chem. Sci.* **2017**, *8*, 6799−6803.
(44) Lee, B.; Moon, D.; Park, J. Microscopic and mesoscopic dual postsynthetic modifications of metal-organic frameworks. *Angew. Chem., Int. Ed.* **2020**, *59*, 13793−13799.
(45) Qi, S.-C.; Qian, X.-Y.; He, Q.-X.; Miao, K.-J.; Jiang, Y.; Tan, P.; Liu, X.-Q.; Sun, L.-B. Generation of hierarchical porosity in metal-organic frameworks by the modulation of cation valence. *Angew. Chem., Int. Ed.* **2019**, *58*, 10104−10109.
(46) Qin, Y.; Han, X.; Li, Y.; Han, A.; Liu, W.; Xu, H.; Liu, J. Hollow mesoporous metal-organic frameworks with enhanced diffusion for highly efficient catalysis. *ACS Catal.* **2020**, *10*, 5973−5978.

https://doi.org/10.1021/acscentsci.1c00743
ACS Cent. Sci. 2021, 7, 1434−1440

(47) Yang, P.; Mao, F.; Li, Y.; Zhuang, Q.; Gu, J. Hierarchical porous Zr-based MOFs synthesized by a facile monocarboxylic acid etching strategy. *Chem. - Eur. J.* **2018**, *24*, 2962−2970.
(48) Kim, M.; Cahill, J. F.; Fei, H.; Prather, K. A.; Cohen, S. M. Postsynthetic ligand and cation exchange in robust metal-organic frameworks. *J. Am. Chem. Soc.* **2012**, *134*, 18082−18088.
(49) Shearer, G. C.; Vitillo, J. G.; Bordiga, S.; Svelle, S.; Olsbye, U.; Lillerud, K. P. Functionalizing the defects: postsynthetic ligand exchange in the metal organic framework UiO-66. *Chem. Mater.* **2016**, *28*, 7190−7193.
(50) Taddei, M.; Wakeham, R. J.; Koutsianos, A.; Andreoli, E.; Barron, A. R. Post-synthetic ligand exchange in zirconium-based metal-organic frameworks: beware of the defects! *Angew. Chem., Int. Ed.* **2018**, *57*, 11706−11710.
(51) Boissonnault, J. A.; Wong-Foy, A. G.; Matzger, A. J. Core-shell structures arise naturally during ligand exchange in metal-organic frameworks. *J. Am. Chem. Soc.* **2017**, *139*, 14841−14844.
(52) Wu, W.; Su, J.; Jia, M.; Li, Z.; Liu, G.; Li, W. Vapor-phase linker exchange of metal-organic frameworks. *Sci. Adv.* **2020**, *6*, No. eaax7270.
(53) Cavka, J. H.; Jakobsen, S.; Olsbye, U.; Guillou, N.; Lamberti, C.; Bordiga, S.; Lillerud, K. P. A new zirconium inorganic building brick forming metal organic frameworks with exceptional stability. *J. Am. Chem. Soc.* **2008**, *130*, 13850−13851.
(54) Furukawa, H.; Gandara, F.; Zhang, Y.-B.; Jiang, J.; Queen, W. L.; Hudson, M. R.; Yaghi, O. M. Water adsorption in porous metal-organic frameworks and related materials. *J. Am. Chem. Soc.* **2014**, *136*, 4369−4381.
(55) Loiseau, T.; Serre, C.; Huguenard, C.; Fink, G.; Taulelle, F.; Henry, M.; Bataille, T.; Férey, G. A rationale for the large breathing of the porous aluminum terephthalate (MIL-53) upon hydration. *Chem. - Eur. J.* **2004**, *10*, 1373−1382.
(56) Taking into consideration the volume limit of the flask available in our laboratory (1 L), we have tried 10 g of MOF conversion with 800 mL of aqueous solvent to prove the feasibility toward large-scale conversion in one pot, but we believe that such a reflux-assisted process is very easy to scale up to a higher mass if performed in a larger-volume reactor.
(57) Gong, Y.-N.; Zhong, W.; Li, Y.; Qiu, Y.; Zheng, L.; Jiang, J.; Jiang, H.-L. Regulating photocatalysis by spin-state manipulation of cobalt in covalent organic frameworks. *J. Am. Chem. Soc.* **2020**, *142*, 16723−16731.
(58) Lu, Z.; Liu, J.; Zhang, X.; Liao, Y.; Wang, R.; Zhang, K.; Lyu, J.; Farha, O. K.; Hupp, J. T. Node-accessible zirconium MOFs. *J. Am. Chem. Soc.* **2020**, *142*, 21110−21121.
(59) Feng, D.; Gu, Z.-Y.; Li, J.-R.; Jiang, H.-L.; Wei, Z.; Zhou, H.-C. Zirconium-metalloporphyrin PCN-222: mesoporous metal-organic frameworks with ultrahigh stability as biomimetic catalysts. *Angew. Chem., Int. Ed.* **2012**, *51*, 10307−10310.
(60) Cai, G.; Yin, Y.; Xia, D.; Chen, A. A.; Holoubek, J.; Scharf, J.; Yang, Y.; Koh, K. H.; Li, M.; Davies, D. M.; Mayer, M.; Han, T. H.; Meng, Y. S.; Pascal, T. A.; Chen, Z. Sub-nanometer confinement enables facile condensation of gas electrolyte for low-temperature batteries. *Nat. Commun.* **2021**, *12*, 3395.
(61) Ding, M.; Flaig, R. W.; Jiang, H.-L.; Yaghi, O. M. Carbon capture and conversion using metal-organic frameworks and MOF-based materials. *Chem. Soc. Rev.* **2019**, *48*, 2783−2828.
(62) He, H.; Perman, J. A.; Zhu, G.; Ma, S. Metal-organic frameworks for CO_2 chemical transformations. *Small* **2016**, *12*, 6309−6324.
(63) Lu, X.-B.; Darensbourg, D. J. Cobalt catalysts for the coupling of CO_2 and epoxides to provide polycarbonates and cyclic carbonates. *Chem. Soc. Rev.* **2012**, *41*, 1462−1484.

https://doi.org/10.1021/acscentsci.1c00743
ACS Cent. Sci. 2021, 7, 1434−1440